

## Application of mean statistics derived from Sentinel-1 time series on forest – examine forest type and correlation with biomass layers

Zlatomir Dimitrov

Space Research and Technology Institute – Bulgarian Academy of Sciences  
e-mail: zlatomir.dimitrov@space.bas.bg

**Keywords:** Sentinel-1, time series, forest, RVI, SAR indices, CCI-Biomass, GlobBiomass, pyroSAR

**Abstract:** This study is focused on the mean characteristics derived from Sentinel-1 time series, on mountainous forest in Bulgaria, for a four year period of continuous observation. General aim is to demonstrate the utilization of resulted SAR observables in C-band by means of dual polarimetry, in mountainous disturbed forest, along the diversity of forest layer and local incidence angle. To study also statistical relationship between the SAR observables and forest parameters. The SAR observables consists of statistical mean values of both VH and VV backscatter intensities, and the dual-pol Radar Vegetation Index (dRVI). Three layers describing forest parameters are used as dependent variables, where - GlobBiomass-2010© and CCI-Biomass-2018©, freely provided by University of Jena (Lehrstuhl für Fernerkundung), and also Tree-Cover-Density-2015 in the scope of COPERNICUS Services. Time series processing is performed within the OS framework “PyroSAR”, developed there. Disturbed forest is considered, resulted from past Icethrow disaster event. Various RGBs are calculated, in order to distinguish particular backscatter behavior related to different conditions. Particular SAR responses are summarized for mean - dRVI, VH and VV, and used for supervised classification using SVM. Forest type and Forest/Non-forest masks are resulted from SVM-classifications, where highest accuracy achieved is 78%, whereas about forest masks highest accuracy is 91%. Additional SAR indices - such as dual-pol SAR Vegetation Index (dSVI) and Polarization Ratio (PR) are also calculated, showing non-significant contribution. Performed regression analysis shown that none significant correlation is observed between the SAR observables and biomass layers in mountainous forest. Nonetheless, high correlation exists between dRVI and local incidence angle, with  $R^2 = 0.78$ . Therefore, the mean characteristics calculated from the Sentinel-1 C-band using time series approach, show good feasibility to study forest areas. This study was kindly supported by Prof. C. Schmullius, PhD F. Cremer, Dr. N. Salepci from FSU-Jena, Lehrstuhl für Fernerkundung, in the framework of ERASMUS+ Programme.

## Приложение на средни стойности на времева серия от Sentinel-1 в гори в планински територии – определяне вида на гората и статистическа корелация със слоеве биомаса (GlobBiomass, CCI-Biomass, TCD)

Златомир Димитров

Институт за космически изследвания и технологии – Българска академия на науките  
e-mail: zlatomir.dimitrov@space.bas.bg

**Ключови думи:** Sentinel-1, времева серия, гори, RVI, CCI-Biomass, GlobBiomass, TCD, pyroSAR

**Резюме:** Това изследване е фокусирано върху приложение на средни стойности на характеристики, получени от времева серия от радари със синтезирана апертура (SAR), от – Sentinel-1. Основната цел на настоящия доклад е да се демонстрира потенциалът на продължителните измервания в микровълнов канал „C“, за изследване на горски територии от различен тип в планински район. От средните стойности на обратното разсейване (VH и VV) е изчислен Радарния индекс на растителността – RVI, където в три-канална комбинация е изследван обратния отговор от различни видове обекти. Изчислени са и други два индекса – SVI и Polarization ratio, с цел да се провери техния принос в изследването. Основен проблем се явяват геометричните дефекти в радарното изображение. Извършени са неконтролируеми (ISO Cluster) и контролируеми (SVM) класификации, показвайки различна точност, като е изчислена и маска на горската растителност. От направения Principal Component Analysis са разпознати различни обекти отнесени към вида на гората и други класове земно покритие. От друга страна, в доклада се изследва статистическата сходимост между изчислените характеристики от Sentinel-1 и слоеве за състоянието на гората. Това са - GlobBiomass-2010© и CCI-

*Biomass-2018*© предоставени от Университета в Йена, както и *Tree-Cover-Density-2015*© в рамките на COPERNICUS Services. Времевата серия е изчислена със софтуерни продукти на Университета в Йена. Проведения корелационен анализ не показва статистическа сходимост, между характеристиките от Sentinel-1 и слоевете биомаса. Въпреки това, се наблюдава корелация между dRVI и локалния ъгъл на падане, където  $R^2 = 0.78$ . Направеното изследване показва голям потенциал за изследване на горски територии, чрез времева серия от Sentinel-1. Това изследване е подпомогнато с данни и софтуер от Университета в Йена (FSU-Jena), Lehrstuhl für Fernerkundung, в рамките на обмен по програма ЕРА3ЪМ+.

## Introduction

Forests have been widely studied with SAR via variety of methods and techniques, which overcome a lot of imitations that frustrates optical approaches [1]. By means of e.m. properties of the backscattered chirp (e.g. polarization, intensity and phase), the bio-physical properties of the forest volume could be estimated [2, 3]. Forest parameters estimation, like the Above Ground Biomass (AGB) and forest stand Height via SAR measurements, are wavelength dependent [2, 4]. Assessed techniques comprises of scalar interferometry (InSAR) and vector interferometry (POLinSAR) that allows modelling of the backscattered signal throughout the forest volume [2, 5, 6]. Besides, measuring polarization states that constitutes of dual- or quad-pol, is of great importance in order to retrieve the geometric properties of the scattering media [7]. Dual polarization instruments that operates in C-band, like Sentinel-1 constellation, are capable to achieve accurately to delineation of the land cover classes [8]. Nonetheless, assessing growing stocks via SAR signal could be limited, due to saturation problems as a function of the wavelength, from which point SAR intensities could not be related with the biomass [9]. A lot of limitations imposed by environmental issues (e.g. precipitation) could be overcome, when assessing SAR intensities approach via time series analysis [10]. Considering forests, time series analysis based solely on SAR intensities is promising to assess forest structure and to delineate broadleaf from coniferous types [11]. In that relation, the ESA Copernicus - Sentinel-1 dual-pol C-band SAR mission offers great perspectives such a forest studies, by means of time series analysis. Dedicated world biomass estimation projects by ESA in the face of *GlobBiomass* and *CCI-Biomass* with referent years of the AGB layers - 2010 and 2018 [11, 12], introduces good basement for biomass change detection. In spite of that uncertainties should be analyzed, related to the local specifics of the landscape and environment, or even disaster events like Icethrow. The COPERNICUS Services – *Tree Cover Density* (TCD-2015) layer brings also fruitful information to the forest condition estimation.

Bulgarian temperate forests have commonly been affected by abiotic disturbance events, such as Icethrow. Due to harsh conditions in the mountains in winter, such massive disaster event happened in the late of 2014, demolishing more than 5 000 Hectares [13]. That brings needs of studying Bulgarian mountainous forests via SAR methods, where time series analysis is of great potential. Currently, there are no such studies in Bulgarian literature, which to assess utilization of Sentinel-1's time series in disturbed forest, especially on the North-West slope of Stara Planina Mountain. It is not studied also correlation of the C-band time series observables, with *GlobBiomass* and *CCI-Biomass* layers.

This study namely considers time series analysis application in Bulgarian temperate forest, resulted from for years of continuous observation, using Sentinel-1 SAR data. Resulted mean values of the backscatter intensities - VH and VV are used to calculate the dual-pol Radar Vegetation Index (dRVI). The dRVI have proven its potential in vegetation structure mapping, related with the optical NDVI [14]. In addition, the SAR vegetation index (dSVI) and Polarization ratio (PR) are also calculated. Two general approaches are followed, where in the first one thematically delineation of the land cover objects is pursued, via RGB combinations of dRVI-VH-VV, and Principal Component Analysis (PCA). Optical data is used for reference, comprising the VHR *GoogleSatellite* base map, and ancillary Sentinel-2 imagery. Resulted are unsupervised and supervised classifications with forest type, and forest/non-forest masks, where accuracy assessment is performed on those products in QGIS. The second approach tests statistical relationship between biomass layers provided from the University of Jena, Lehrstuhl für Fernerkundung – *GlobBiomass-2010* and *CCI-Biomass-2018*, with the Sentinel-1 mean observables from time series. Also, correlation is pursued with the local incidence angle and TCD-2015 from Copernicus Services. The time series calculations from Sentinel-1 data are performed at the FSU-JENA, Lehrstuhl für Fernerkundung, within ERASMUS+ exchange, with the kind support of Prof. C. Schmullius, Dr. N. Salepci and PhD F. Cremer. This study correlates with the Author's PhD study.

## Data used and test site

The Sentine-1 (S1) SAR C-band data were used for time series analysis, in dual polarimetry that constitutes of – VH and VV. The S1 data specification used are summarized in the following table.

Table 1. Sentinel-1A/B SAR data specification, used at test sites – TS20 and TS21

<b>Orbit</b>	Descending	<b>Product type</b>	GRDH
<b>Relative Orbit Number</b>	80	<b>Mean incidence angle</b>	38 deg
<b>Resolution cell</b>	10 m	<b>Azimuth / range looks</b>	5 / 1
<b>Begin / End of acquisition</b>	23th Oct. 2014 / 17th May 2018	<b>Polarization</b>	VH / VV

Time series begins with the first available GRD-SAR image from Sentinel-1A, with benefit of the highest possible 10 m spatial resolution, and firstly having 12-days of temporal resolution. Since October 2016 the Sentinel-1B observations contribute to the time series, which improved the temporal resolution up to 6 days. Total period of continuous observation is four years. The SAR data is extracted via API-Hub of the Open Access Data Hub, by using the software tool developed at the University of Jena – “esa\_sentinel\_api“, by Jonnas Erlebe and John Truckenbrodt. Preliminary analysis pointed out that Sentinel-1’s Relevant Orbit Number – 80 suits to the desired test area, which covers test sites – TS20 and TS21, from the Author’s PhD. Projections used are - World WGS84 (4326), or UTM 34N (32634)

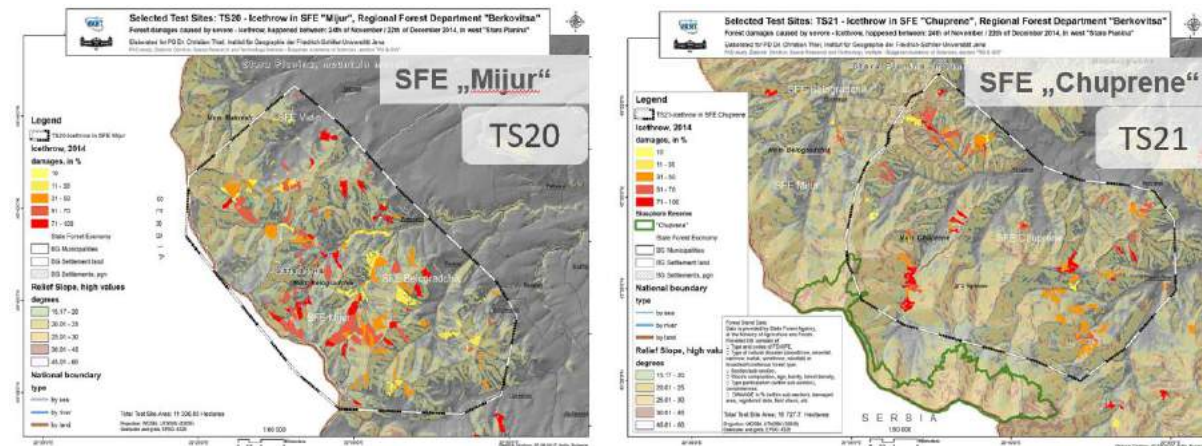


Fig. 1. Test sites maps, of - TS20 in SFE "Mijur" and SFE "Chuprene", with forest disturbances patches from 10% up to 100% forest loss, from the past Icethrow event in 2014, are overlaid on the DEM slope map

The test sites - TS20 and TS21 are located near North-West slope of the Stara Planina Mountain massif, in the vicinity of the State Forest Entities (SFE) of “Mijur” and “Chuprene” respectively. Severe natural disaster - Icethrow happened in late December 2014 erasing whole stands, with damages up to 100% at SFE “Mijur. The total affected area was about 50 000 Decares of century-old forest [11]. Test site maps of TS20 and TS21 are prepared using reference database for forest disturbances, according to the author’s PhD study, showing stands with damages from 10 to 100% (Fig. 1). Species distribution charts are elaborated according to the forest plans, where TS20 showed – 88.8% broadleaf forest, contrary to - 11.2% for coniferous one. About TS21, the broadleaf forest is – 72.4%, contrary to - 27.6 for coniferous, thus TS21 shows more coniferous forest unlike TS20. In spite of that, many forest stands were with undetermined tree species in the forest plans, hence was marked out with “no data” (Fig. 2).

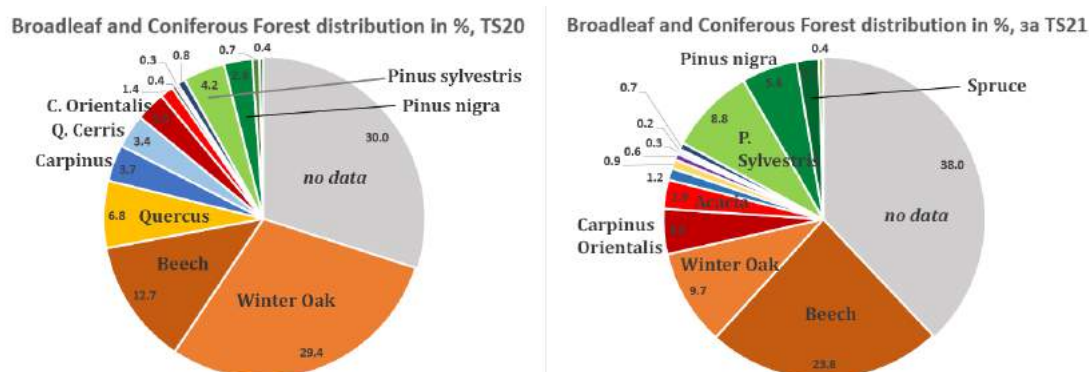


Fig. 2. Tree species distribution on TS20 and TS21, represented in %. Significant percentage of forest stands are with tree species undetermined - e.g. "no data". The TS21 is much coniferous type, rather than TS20.

Reference biomass data is represented by layers - *GlobBiomass-2010* and *CCI-Biomass-2018*, exclusively provided by Friedrich-Schiller-Universität - JENA, Institut für Geographie, Lehrstuhl für Fernerkundung. Resolution cell of both raster datasets is 90 m, where the CCI-Biomass layer originally

may have had coarser spatial resolution, in regard to the GlobBiomass one (Fig. 3). Auxiliary layer – Tree-Cover-Density – 2015 freely accessed from COPERNICUS Services is also incorporated, coming with spatial resolution of 20 m, in order to test its correlation with Sentinel-1 SAR observables.

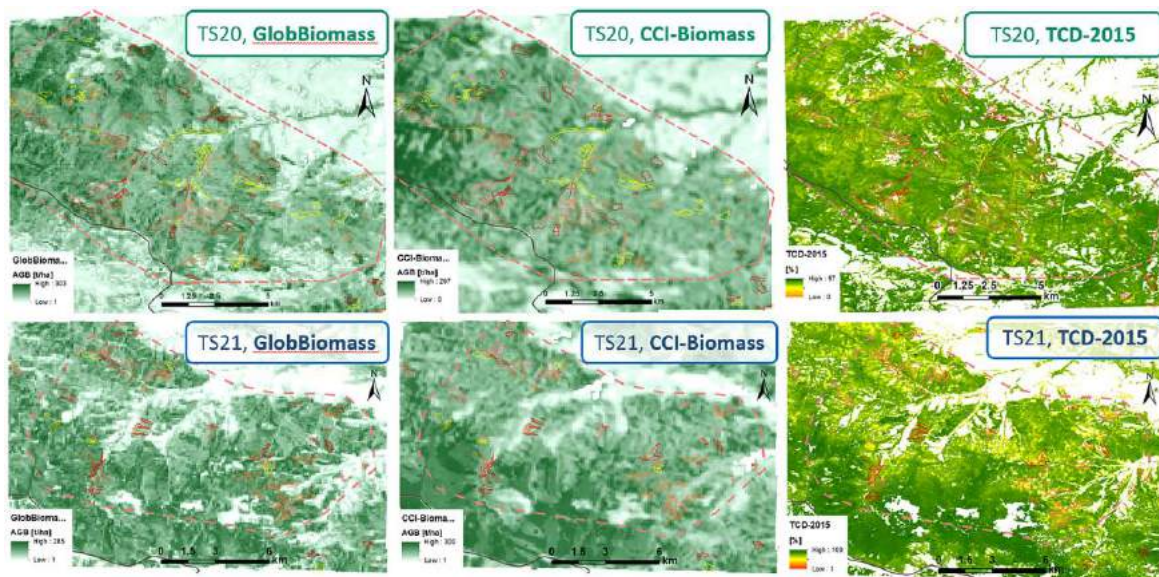


Fig. 3. Raster datasets representing AGB, exclusively provided by FSU-Jena (Lehrstuhl für Fernerkundung) - GlobBiomass-2010 and CCI-Biomass-2018, as well as Tree-Cover-Density-2015 from COPERNICUS Services.

Reference optical imagery used are the VHR *GoogleSatellite*© base map, and Sentinel-2 from 6<sup>th</sup> Oct., 2018, with id: [S2B\\_MSIL2A\\_20181006T092029\\_N0208\\_R093\\_T34TFP\\_20181006T142726](https://earthengine.googleapis.com/v2/projects/sentinel2a/datasets/S2B_MSIL2A_20181006T092029_N0208_R093_T34TFP_20181006T142726). Whole bands are resampled, spatial resolution is 10 m. The RGB used is: B8 (842nm) – B5 (705nm) – B3 (560nm).

## Methodology

The methodology is based on time series approach that aims direct interpretation of the mean values of Sentinel-1 GRD data, with benefit of dual polarization states of VH and VV. Methodology also aims utilization of the dual-pol Radar Vegetation Index (dRVI) in respect to diversity of the temperate mountainous forest; calculation is performed using the following formula [14]:

$$(1) \quad dRVI = \frac{4\sigma_{vh}^0}{\sigma_{vv}^0 + \sigma_{vh}^0}$$

General steps are: download of the Sentinel-1 GRD data, geocode and time series generation; calculation in Python of mean values from time series for - VH, VV and dRVI (formulating *S1-mean-characteristics* of the mean backscatter); calculation of the additional - dSVI and Pol. Ratio are followed up. First approach in methodology considers thematic analysis in GIS with two RGBs – RGB-1 (dRVI-VH-VV), RGB-2 (SVI-PR-dRVI) and Principal Component Analysis (PCA), where to analyze particular contribution of the characteristics; summary and classification of distinct land-cover type is made, referenced by VHR base map of *GoogleSatellite*© and Sentinel-2 satellite imagery. Forest/non-forest masks, as well as forest type are resulted from the supervised classification, followed by accuracy assessment. Second approach tests statistical correlation, which models the local incidence angle, GlobBio, CCI, and TCD, versus the mean SAR-observables in C-band as independent variables (Fig.4).



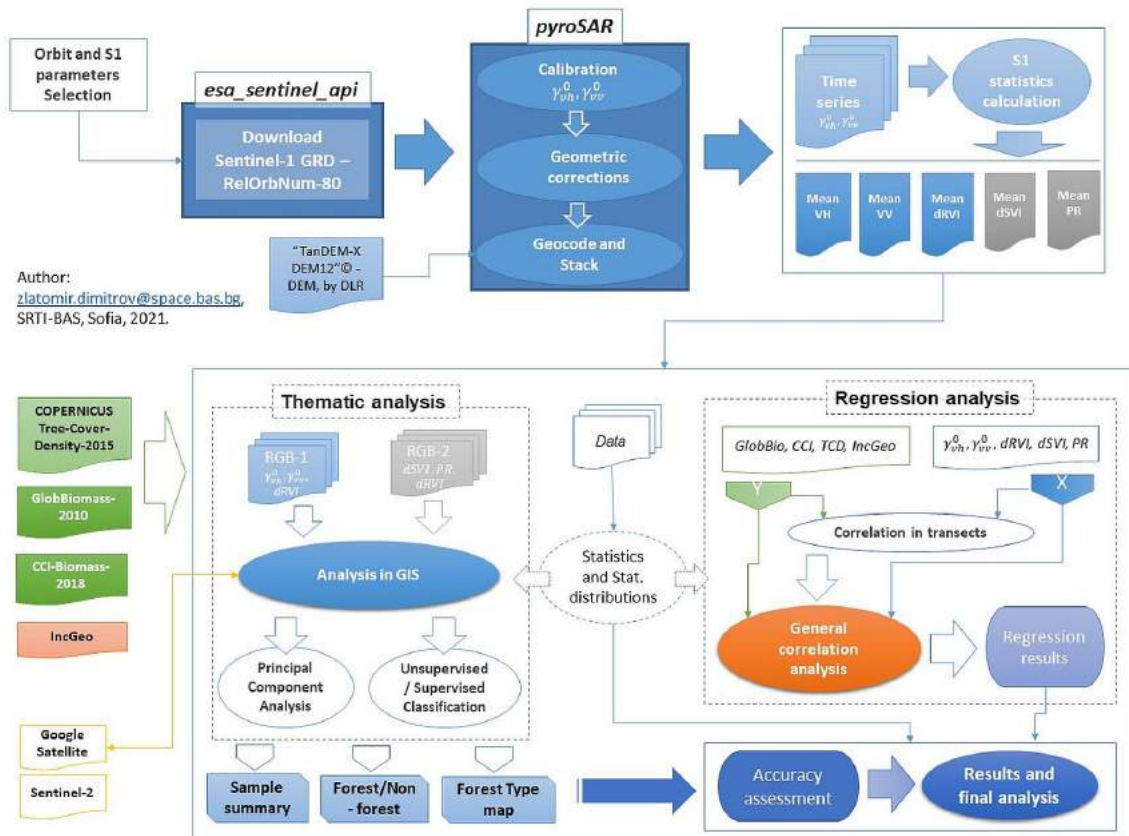


Fig. 4. Workflow chart, representing general steps of the analysis

## Results and Discussion

### S1 - Time series elaboration

Download of the Sentinel-1 GRD products is made via – “*esa\_sentinel\_api*” tool developed at the University of Jena, by J. Erlebe and J. Truckenbrodt in the framework of ESA project. Desired test site boundaries are applied, where download is performed via the ESA Copernicus Open-Access / API Hub. A total amount of 138 successfully downloaded scenes is achieved in “Descending” orbit from 158 available ones at the Hub. The “missing data” or broken archives are especially in the beginning of the Sentinel-1A lifecycle, as seen on Fig. 5. After downloading, for each pixel the Ellipsoidal ( $E$ ) radar cross section by means of *gamma-nought* ( $\gamma^0$ ) is calculated, from *sigma nought* ( $\sigma^0$ ) and incidence angle -  $\theta_i$ :

$$(2) \quad \gamma_E^0 = \sigma_E^0 / \cos\theta_i$$

A topographic normalization is used to derive terrain flattened intensities, based on the method proposed by D. Small [16], which is needed due to rugged terrain in the test areas. Whole of that is done during the geocoding of GRD-data, which is made in the framework of “*pyroSAR*” using the - SENTINEL-API, by function - *geocode()*. The SENTINEL-API uses ESA SNAP implemented geocoding methods.

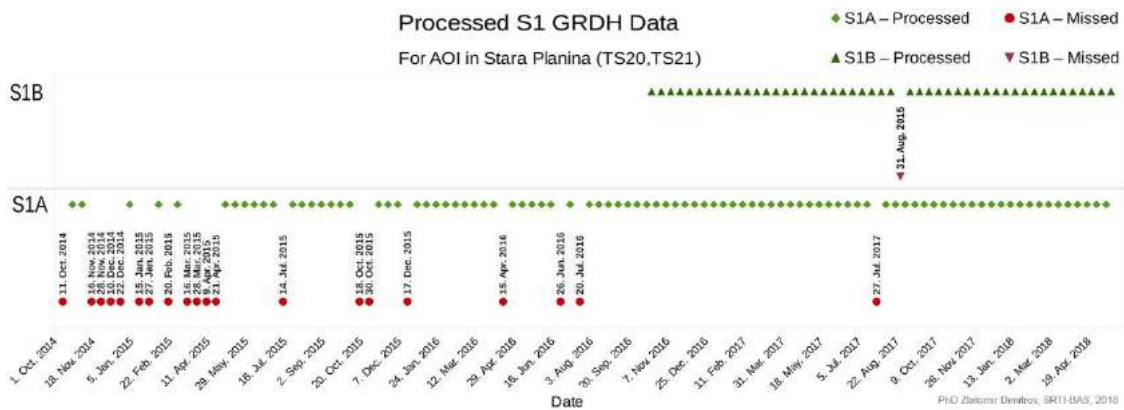


Fig. 5. Sentinel-1A/B available and successfully downloaded GRD data scenes that covers both test sites. From total amount of - 158, a 138 have been successfully downloaded and processed.

The *pyroSAR* is a Python based extensive framework, which includes wide toolset and APIs for SAR imagery manipulation and processing, developed at the University of Jena (FSU-JENA), Institut für Geographie, Lehrstuhl für Fernerkundung [17]. At the geocoding, the highly scaled reference DEM – “TanDEM-X DEM12”© provided by DLR, is used, in the frame of “DEM Proposal”. Afterwards, a stack of geocoded data via “*pyroSAR*”, using – *stack()* is elaborated, for each polarization, using ENVI file container, with BSQ order in a 32-bit pixel depth. Thereafter the mean values from times series ( $\gamma_{vv}^0, \gamma_{vh}^0, \overline{dRVI}$  – *S1-mean-characteristics*) are calculated in Python, for both test sites – TS20/TS21 (Fig. 6).

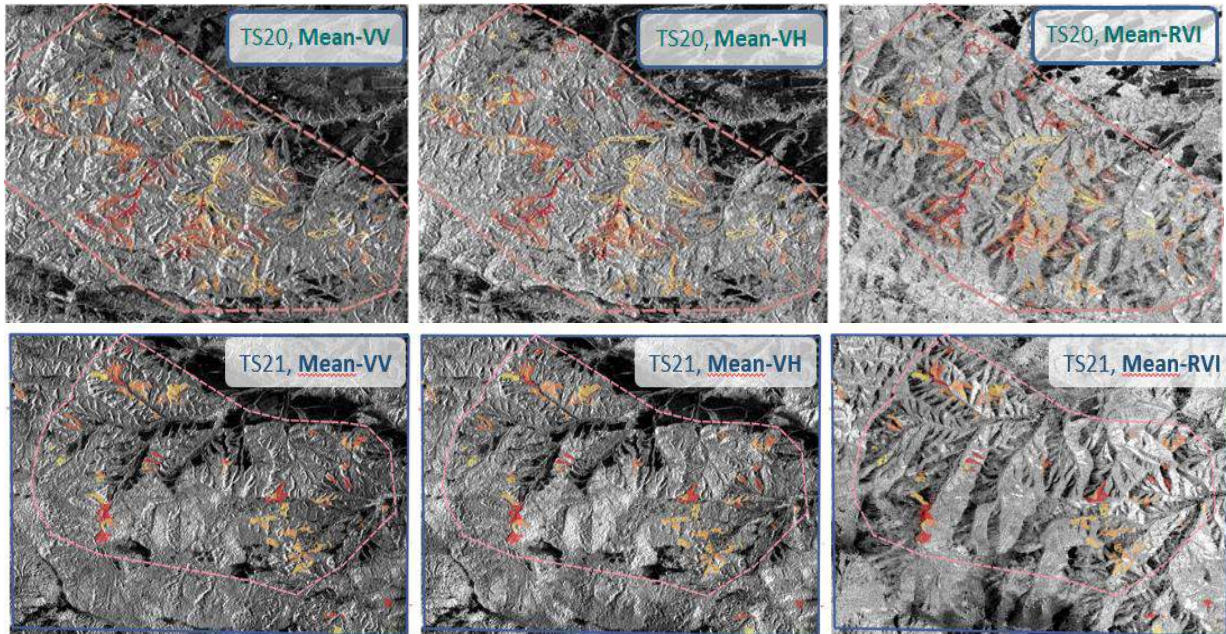
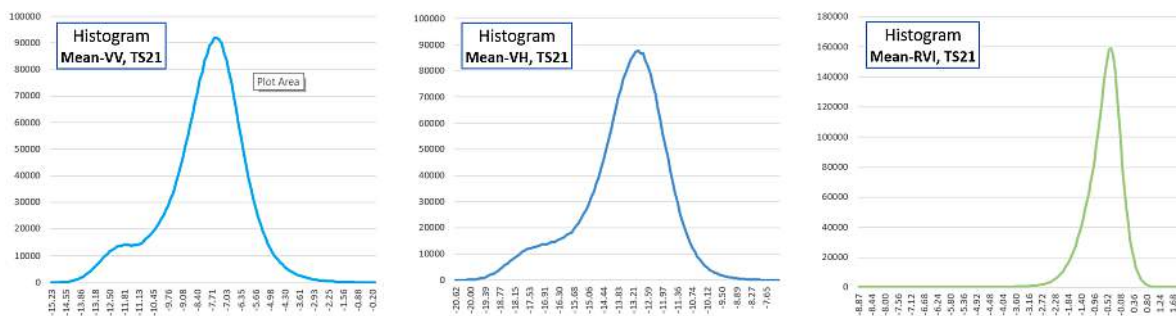


Fig. 6. Mean values from S1-time series, where from left to right are -  $\gamma_{vv}^0, \gamma_{vh}^0$ , and  $\overline{dRVI}$ , for TS20 and TS21

Statistics are calculated for each dataset, representing statistical distribution of the mean backscatter on different S1-characteristics, over the test areas of TS20 (SFE “Mijur”) and TS21 (SFE “Chuprene”) - Fig. 7.





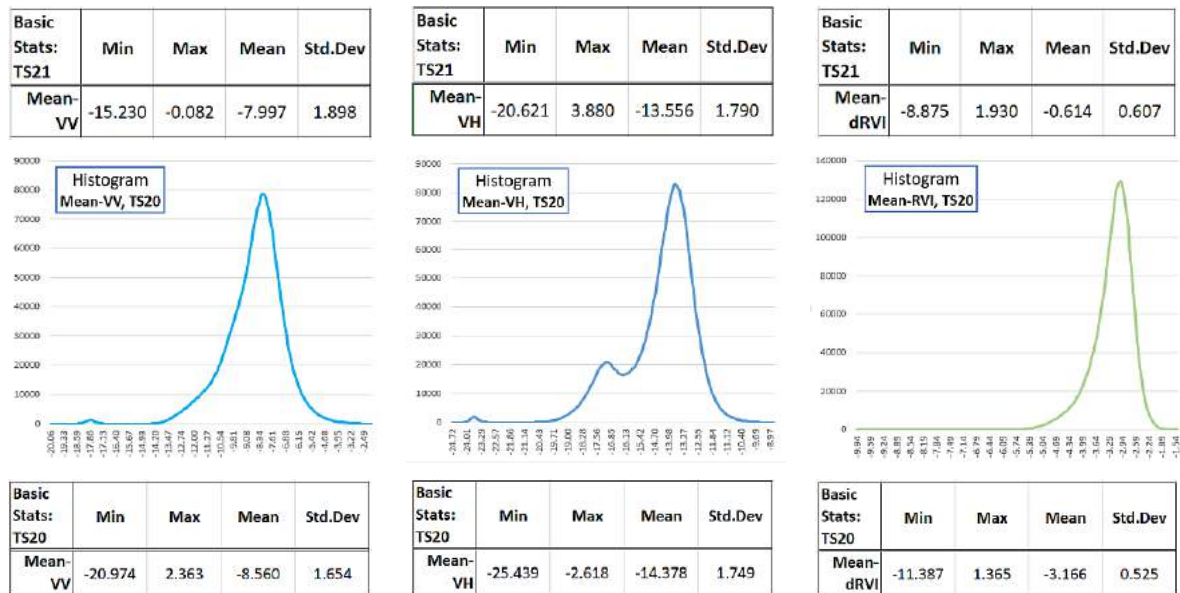


Fig. 7. Statistics and histograms of the calculated S1-characteristics for TS20 and TS21, using Decibel scale

Statistics on Fig. 7, confirms lower mean of the cross-pols ( $\overline{\gamma_{vh}^0}$ ) rather than the co-pols ( $\overline{\gamma_{vv}^0}$ ), with more than 6 dB, due to volumetric backscatter. Histogram profiles of S1-characteristics doesn't look very similar for both test sites, except the dRVI distributions. The only difference here is in the range of the values, where at the TS20, the dRVI show higher response. Also, notable is the standard deviation of the dRVI versus polarizations, which is one third of the VH and VV. Besides, the cross-pol for TS20 shows little extremum near -17 dB. Reason for that as founded, belongs to the agricultural areas in the NE part of the scene. Maximums of both polarizations encompass backscatter from forest areas, where different histogram profiles of TS20 and TS21 are dedicated to the complexity of the landscape.

On the other hand, from the calculated mean values of S1-time series (Fig. 6) following is observed: 1) the speckle noise is missing; 2) relief affects differently the three S1-characteristics, where on the  $\overline{\gamma_{vv}^0}$  foreshortenings are more obvious (bright stripes), rather than the  $\overline{\gamma_{vh}^0}$ . This is because the  $-\overline{\gamma_{vh}^0}$  is more sensitive to the forest volume, despite the response from  $-\overline{\gamma_{vv}^0}$  that comes mainly from phase centers located in the crowns. That results to dark areas on  $\overline{dRVI}$  in forest, corresponding to geometric distortions – foreshortenings. Those areas are related with low local incidence angles between target vector and the radar beam, below 29 deg. Therefore, dRVI seems to be very sensitive to the relief; 3) The dRVI “sinks” over forest area, but shows higher values over grassland, crops, water, and random over bare/urban areas. Specific interestingly, the dRVI shows lower values on South at TS21, over the Biosphere Reserve (BR) “Chuprene”, characterized with dense and lower height coniferous species.

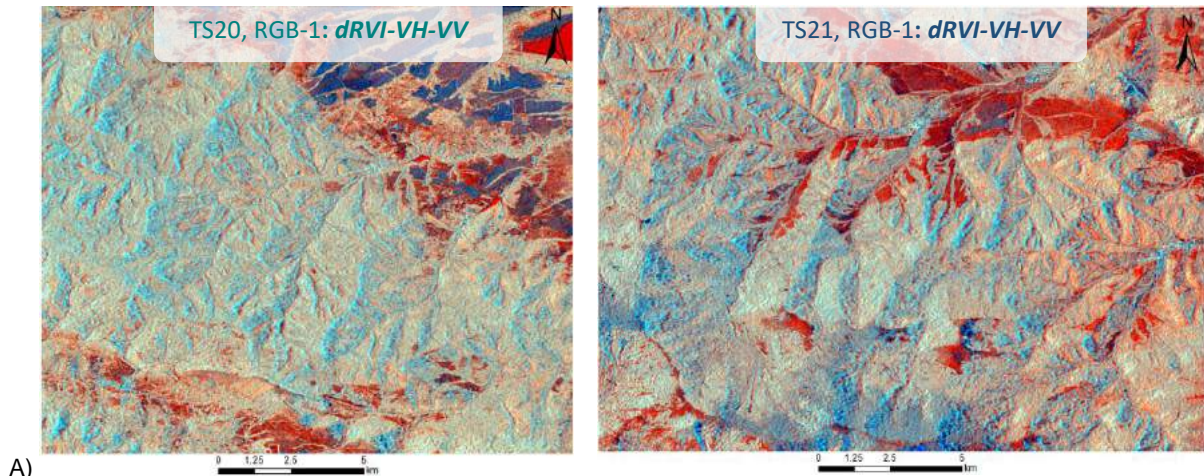
### Thematic analysis, by means of S1-mean-characteristics

First approach pursue utilization of the RGB-1: dRVI-VH-VV, which underlines well backscatter contribution in respect to the type of land cover objects (see, fig. 8). Discussed dependencies above are clearly observed on RGB1, over TS20 and TS21, where more peculiarities are recognized. As seen from Fig. 8, the dark-red regions belong to grassland, some crops and standing water body; dark-blue belongs to other crops and bare fields; in light-blue mainly foreshortenings are recognized. Forest is colored from bright-beige colors, through orange patches and ends up with bluish that's belongs to the dense coniferous forest of BR “Chuprene” on TS21. Analysis shows that general reason for color changing in forest is dedicated to the dRVI. To track out those changes as eigen-based approach, a Principal Component Analysis (PCA) is calculated from the RGB-1. Herewith the PCA, forest structure is distinctly recognized, where wine-reddish and greenish regions give imprint amongst the rest of the pixels. Green areas are related to foreshortenings, while magenta colors reveal non-forest areas.

Those relations are tracked out in GIS by using the VHR optical base map of *GoogleSatellite*. The wine-red areas at the PCA-1 that shows up as dark-orange at RGB-1, resulted as a coniferous forest patches. Those areas exhibits high values in dRVI, above -2.5 dB, but mixed up with values over water and crops. That means that the dual-pol RVI brings up precious contribution, to differentiate forest type in C-band SAR! Overlaying the TCD-2015 (COPERNICUS) and CCI-Biomass-2018 (Uni-JENA) in GIS, showed high values of biomass (above 100 t/ha) and density (above 79%) within those dark-red patches that constitutes of coniferous forest (see, fig. 9). Whilst, analyzing the dense forest at the BR “Chuprene” (TS21) via the PCA-1 and biomass layers, showed high biomass (above 250 t/ha) on CCI-

Biomass, and density above 92 %. As stated, the dRVI there shows low values over forest. To obtain more information on this particular forest, the Sentinel-2 L2A reference imagery was used, with date of acquisition – 2018-10-06. Analysis confirmed that this is coniferous forest type, but with rather different spectral signature from the rest of the coniferous forest. Therefore, additional sensitivity of the dRVI to particular coniferous species in high mountain is observed (refer to Fig. 9, and Table-2).

In other hand, none distinct color, or values combination of *S1-mean-characteristics* could be related to the disturbed forest patches. Interestingly, considering forest loss above 80%, the dRVI showed higher values, pointing out to fresh vegetation regrowth. Must be stated also that the dRVI solely could not differentiate forest from non-forest area!



A) Fig. 8. The RGB-1: dRVI-VH-VV, for both test sites - TS20 and TS21, with good representation of the different land cover objects, based on backscatter response, due to sensitivity of the dRVI to vegetation

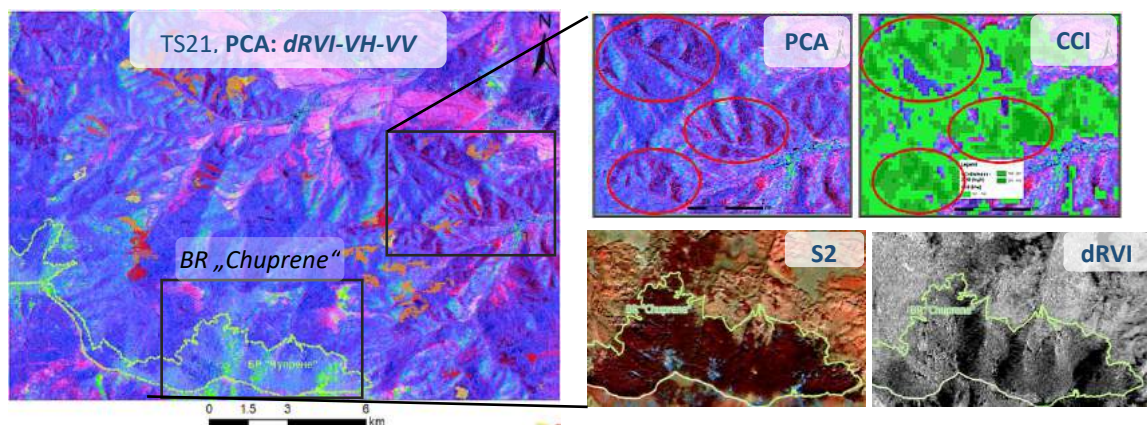


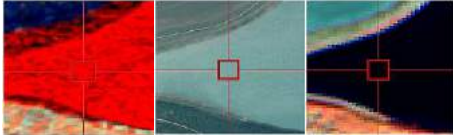






Fig. 9. The PCA-1 for TS21, derived from RGB-1 with disturbed patches and BR "Chuprene" overlaid. On the right: rectangle area, representing: Up - dark-red patches of different forest type/structure that exhibits high biomass (CCI-Biomass); Down – BR "Chuprene" with different coniferous forest, on reference S2 and dRVI.

Samples of land cover objects with different peculiarity are summarized in a table, where the land cover type is confirmed by referring the *GoogleSatellite*© VHR and S2. Also, optical imagery of Sentinel-2 as second reference is used, within RGB of B8(842nm) – B5(705nm) – B3(560nm), see Table-2.

Table 2. Samples of distinct land cover (LC) objects recognized on RGB-1, showing values of  $\overline{\gamma_{vv}^0}$ ,  $\overline{\gamma_{vh}^0}$ , and  $\overline{dRVI}$ , referenced by *GoogleSatellite*© VHR base map, and Sentinel-2 in RGB combination of – B8 - B5 - B3.

RGB-1	Google	S2 - L2A	Samples object in recognized Land Cover (LC) type	$\overline{dRVI}$ [dB]	$\overline{\gamma_{vh}^0}$ [dB]	$\overline{\gamma_{vv}^0}$ [dB]
			Sample 1 – geometric distortions (foreshortennings) over mountainous broadleaf forest (collected from TS20)	-4.163	-10.143	-3.898
			Sample 2 – agricultural fields, or kind of cultivated areas (collected from TS20)	-5.065	-18.086	-9.028



	Sample 3 – standing water body (collected from TS20)	-2.587	-23.653	-17.950
	Sample 4 – grassland / abandoned land, at open forest or non-forest (collected from TS20)	-3.451	-19.372	-13.275
	Sample 5 – coniferous forest type (collected from TS20) *winter VHR image of Google Satellite is used here.	-1.602	-12.833	-8.926
	Sample 6 – broadleaf forest type (collected from TS20)	-2.799	-13.690	-8.342
	Sample 7 – broadleaf mountainous forest on a slope (collected from TS21)	-0.538	-10.673	-5.199
	Sample 8 – second coniferous forest type, in Biosphere Reserve „Chuprene“ (TS21)	-1.894	-14.002	-6.853
	Sample 9 – bare areas, rocks, radar shadows (collected from TS21)	-4.048	-17.569	-7.951

From analysis above is obvious that the foreshortenings totally obstruct interpretation, because of higher sensitivity of the dRVI to geometric distortions. In fact, within certain interval of variations of the local incidence angle (*IncGeo*), the interpretation on slopes is possible; such an example is found on sample-7, where forest is a bit biased, but still interpretable. Other biased interpretation due to *IncGeo* is the top hill bare area with rocks and grass, on sample-9; because of the geometric distortions, firstly grassland is correctly interpreted in reddish, but due to increasing of the local incidence angle, its values become more alike to the agricultural ones, from sample-2.

From the recognized LC - objects above, training samples are elaborated in order to train Supervised classification, using Support Vector Machine – non-parametric machine learning algorithm. Total of eight LC – classes are formulated to classify objects based on the *S1-mean-characteristics* in RGB-1, approached differently in both test sites, represented on table-3. Zonal statistics and histograms are elaborated, about statistical distributions within training zone data, for each class. Largest standard deviation (STD) have classes – 1 (available only in TS21) and 2, in the reason of that they mostly describe geometric distortions, and also because those classes comprises mixture of land cover.

Table 3. Zonal statistics with Standard deviation (STD) of S1-mean-characteristics within training zone data, of classes particular for each test site. \*Grey columns does not belong to the particular classification.

Formulated classes, of the training samples	STD for TS20		STD for TS21	
	Mean-VH	Mean-dRVI	Mean-VH	Mean-dRVI
Class 1 - Radar shadows / Bare area			2.486	1.437
Class 2 - Foreshortenings	1.225	0.332	1.568	0.444
Class 3 - Grassland	0.922	0.336	0.823	0.324
Class 4 - Crops	0.536	0.500	0.640	0.366
Class 5 - Deciduous forest	0.742	0.247	0.938	0.246
Class 6 - Coniferous forest	0.797	0.286	1.008	0.287
Class 7 - Coniferous forest, at BR „Chuprene“			0.817	0.308
Class 8 - Water	0.555	0.238		

The STD for Mean-dRVI in both cases is rather smaller than the mean-backscatter in VH. The STD is quite the same for both training classes – 5 and 6 comprising the deciduous and coniferous forests for both test areas and mean-characteristics, but also and the particular class-7 representing specific coniferous forest type. It should be stated, that the samples were collected over as most as possible homogenous conditions for conifer and deciduous forest (e.g. constant relief, small slope, density, etc.). Here, it was expected that standard deviation of both would defer in the expense of deciduous one, because conifer species are much homogenous, as refer to fig.2, especially for TS21. Nonetheless, rather the opposite is observed comparing STD of the cross-pol (Mean-VH), with largest difference at TS21 in amount of 0.070, in respect to 0.055 for TS20. The reason may be in the mixture of conifer species within the sample and resulting complex volumetric backscatter. The STD for Mean-dRVI is almost equal for both test areas, pointing out for similar coniferous species at TS20 and TS21, as a component of the training samples. Here, considering class-7 containing specific conifer type, the STD for both S1-characteristics is rather higher than regular coniferous in class-6.

Calculated histograms for coniferous training classes are in whole cases non-symmetrical, where for Mean-dRVI in TS20 histogram have strong negative skewness. Whilst, the specific conifer forest in BR “Chuprene” show positive skewness within the histogram. In spite of that, the deciduous class for both test sites are showing almost perfect symmetry. In other hand, sampled Crops showed smaller STD in Mean-VH rather than Grassland, pointing out to more distinct volumetric backscatter. However, the STD of Mean-dRVI is the highest at TS20 (because of the plenty of agricultural fields), and higher than Grassland. The Grassland sampled class-3 showed most symmetrical histograms, along high STD in Mean-VH. Highest STD is observed at class-1, because it encompass samples from bare area, urban and shrubs.

Unsupervised classifications are also elaborated, based on ISO-Cluster, resulted with three particular classes dedicated to forest. Aim is to test differences in accuracy of the resulted classifications and related products. The supervised classifications using SVM approach are shown below, on Fig. 10.

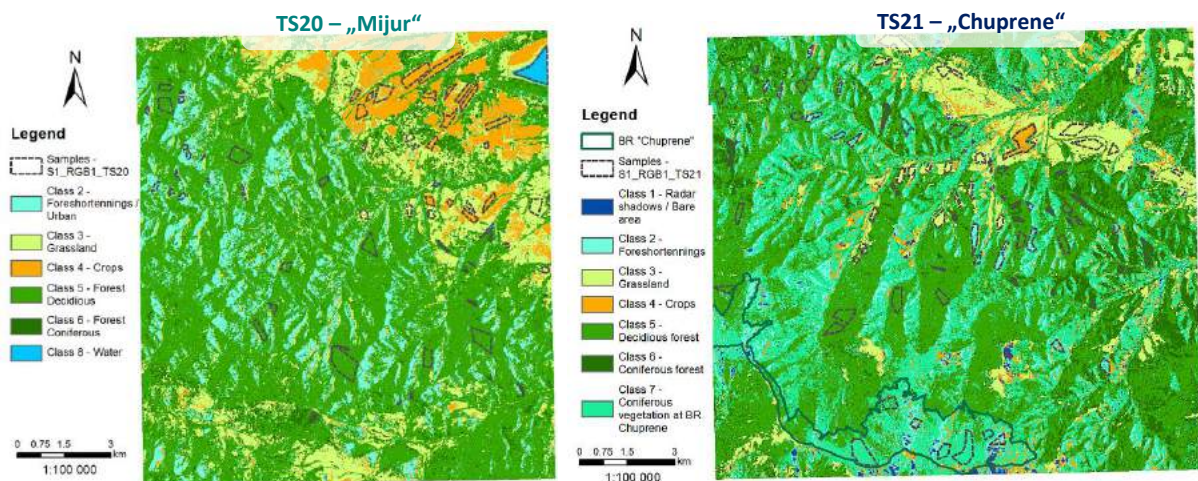


Fig. 10. Supervised classifications, using SVM with same number of classes; training samples are overlaid

The class-2 with foreshortenings comprises much large area on TS21, due to higher relief roughness and incision. Related to that, because of the similarity in values between coniferous forest in BR „Chuprene” and forest in foreshortenings, class-7 comprises large amount of pixels and complement to class-2. That problem does not exist in TS20. Nonetheless, ambiguities persists in particular to the test site and thematic class respectively. Accuracy assessment is therefore performed in order to obtain the Error matrices, including overall accuracy together with the Cohen’s Kappa coefficient, used as a measure of agreement between two individual pixels [18]. Software used is QGIS with the *Semi-Automatic-Classification* (SCP) plugin [19]. For the accuracy assessment of the supervised classifications, 15-random points per class are generated and furtherly validated by the VHR *Google Satellite*© and *Bing World Imagery*© base maps, facilitated by S2-reference imagery. Results from the Error matrices for both supervised classifications are summarized below, in Table-4.

Table 4. Error matrices output summary for both supervised classifications, along thematic classes' accuracy

	Classes	1	2	3	4	5	6	7	8	Overall accuracy [%]	Kappa hat classif.
TS20	PA [%]		94.79	79.99	100.0	89.46	100.0		100.0	78.723	0.6475
	UA [%]		80.0	70.0	80.0	100.0	50.0		100.0		
	Kappa hat		0.78	0.65	0.78	1.00	0.48		1.00		
TS21	PA [%]	9.31	96.21	33.00	100.0	79.31	85.82	100.0		68.897	0.5885
	UA [%]	70.00	80.0	70.0	10.0	100.0	70.0	30.0			
	Kappa hat	0.68	0.79	0.63	0.10	1.00	0.66	0.24			

As seen from table-4, the overall accuracy is higher for test site-TS20. The class-2 have very high Kappa-hat for both classifications, of which resulted very good delineation of foreshortenings. In other hand, the highest Kappa-hat is for deciduous forests. Errors for this class are observed in two directions – enlargement of the forest edge due to sparse forest areas and higher shrubs, and misclassification of urban areas that is specific for rural areas in Bulgaria, where houses are surrounded by lot of trees, especially for abandoned houses, which are very often picture unfortunately in the North-West Bulgaria. Coniferous forest have lower accuracy in respect to deciduous forest, which is more prominent on TS20, because there coniferous types are much less. Moreover, the coniferous types here are mixed up with other forest. Besides, in TS21 conifer patches are more homogenous and better distinguishable. There is no doubt that water is best classified, because of the highest values in dRVI and lowest in cross-pols. In crops class, for TS21 accuracy is very low, due to very small agriculture areas, in respect to the TS20. The grassland class is well classified by means of S1-characteristics.

Comparing supervised with the unsupervised classifications, general conclusion is that coniferous forest could not be delineated and is misclassified as deciduous one. Besides, whole three classes depicts forest areas. In spite of that, better performance of unsupervised classification is observed, in delineation of the forest edge in sparse forest areas (Fig. 11). Also, errors on the supervised on TS20, related to misclassification of agricultural lands as a forest, at unsupervised they are relatively small. Sparse forest is better classified here, but mixed up with shrubs and grassland. Agricultural lands are very well classified on both classifications types.

Resulted products from supervised/unsupervised classifications are - Forest type maps, related to deciduous / coniferous forest types, and Forest/Non-Forest masks, shown below (Fig. 11).

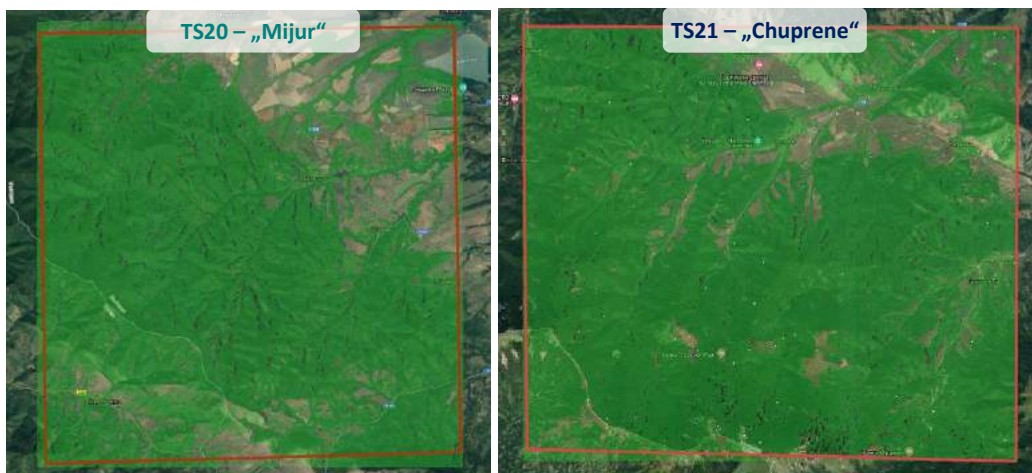


Fig. 11. Forest/Non-Forest masks derived from supervised classifications, where - left: TS20, right: TS21, over Google Satellite© VHR base map

Differences between forests masks approached via supervised or unsupervised classification are very small. Nonetheless accuracy assessment is approached also here, by generation of 60 points – 30 by 30 about forest/non-forest classes. Validation is performed again within QGIS environment, via SCP-plugin, incorporating Google Satellite© base map and Sentinel-2 optical imagery; see Table-5.



Table 5. Error matrices summary of Forest/Non-Forest Masks, derived from Supervised and Unsupervised classifications

	TS20				TS21			
	Supervised		Unsupervised		Supervised		Unsupervised	
	Non-Forest	Forest	Non-Forest	Forest	Non-Forest	Forest	Non-Forest	Forest
<b>PA [%]</b>	74.83	95.38	82.33	93.56	63.53	97.62	100.00	81.35
<b>UA [%]</b>	86.93	90.22	86.78	91.16	87.34	91.21	61.18	100.00
<b>Kappa hat</b>	0.816	0.664	0.800	0.739	0.841	0.571	0.498	1.000
<b>Overall accuracy [%]</b>	89.39		89.75		90.63		85.59	
<b>Kappa hat classif.</b>	0.732		0.769		0.680		0.665	

In overall, whole forest masks have very high accuracy, with high Kappa-hat classification value, showing strong similarity. Differences in accuracy between supervised and unsupervised approaches could be neglected. Highest accuracy is for Forest/Non-Forest mask in TS21 derived from supervised classification, where non-forest class has highest similarity by means of the Kappa-hat. Considering mask elaboration, foreshortenings touching forest at supervised classifications are incorporated, in order to fulfil holes in sloped forest. This is not wrong within current test areas, because mostly geometric distortions are located in mountainous forest areas, rather over bare sloped area. Nonetheless, errors are observed at TS21 in NE direction, where in the sake of misclassification within supervised approach, hills covered with shrubs that exhibits small incidence angles toward SAR antenna, are recognized as forest class-7 that is merged into deciduous and coniferous classes, in order to derive the output mask. In spite, interruptions within forest at both test sites, are due to misclassified forest as grassland or crops. In the forest masks by means of unsupervised approach, foreshortenings are not included because of ambiguities, in spite of that the forest edge is much better delineated (Fig. 12).

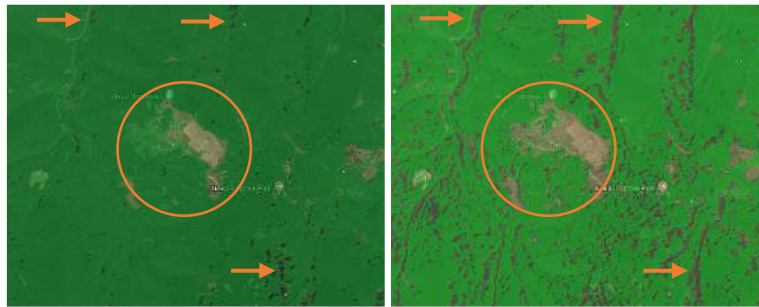


Fig. 12. Comparison in details, between forest masks derived from supervised (left), and unsupervised classification (right), for TS21 in high mountains, near BR “Chuprene” and hut - Gorski Rai

### Additional SAR indices

Complementary SAR indices to the dRVI have been also calculated, based on their functional contribution to describe phenology of crops, mentioned in the literature [14]. Therefore, the dual-pol SAR Vegetation Index (dSVI) and Polarization ratio (Pol.R) are utilized in that study, where to test their functionality into forest status, using equation – 3:

$$(3) \quad Pol.ratio_{cross-pol} = \frac{\gamma_{VH}^0}{\gamma_{VV}^0}; \quad SVI_{dual-pol} = \frac{\gamma_{VH}^0 + \gamma_{VV}^0}{\gamma_{VV}^0}$$

Based on the first approach RGB-2-combination is hereof calculated, based on:  $dRVI$ ,  $dSVI$  u  $Pol.R$ , calculated from the  $S1$ -mean-characteristics -  $\overline{\gamma_{vv}^0}$ , and  $\overline{\gamma_{vh}^0}$ . The GIS analysis showed high correlation in between in the forest territory, with no difference with the dRVI. Thus, in forest high values (white patches) on dSVI and PR are related with coniferous type, whilst forest in BR “Chuprene” is again well delineated (dark grey). Histograms show symmetrical distribution, with small differences in standard deviation, which should be due to diversity in agriculture and forest type (Fig. 13).

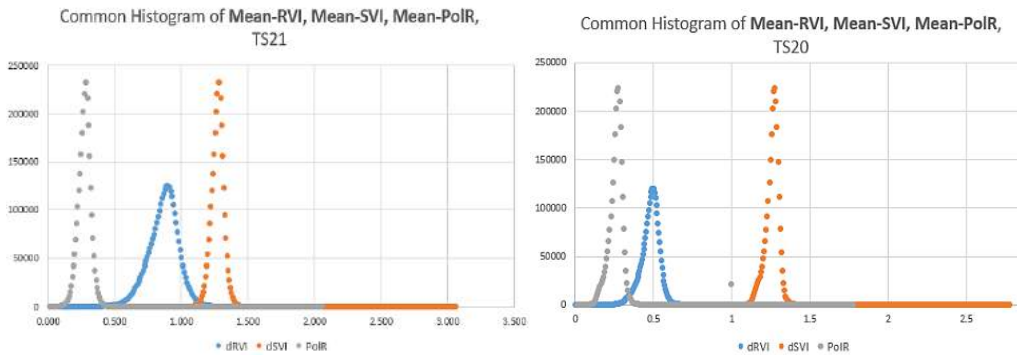


Fig. 13. Common histograms for distribution of the mean values of - dRVI, dSVI and Pol.R., for both test sites

Main differences are observed over agricultural areas, where values of the indices differ in general. On the second PCA calculated from RGB-2, eigen values have almost constant difference in forest area, where:  $\lambda_1 \approx 1.5$ ,  $\lambda_2 \approx 0.5$ ,  $\lambda_3 \approx 0.7$ . Exceptional cases are over some urban pixels (in green and yellow), and some pixels with strong backscatter toward sensor (in yellow) in the mountain; the radar shadows/bare areas from class-1 (RGB-1) are also delineated (in green), see Fig. 14. In the first case where yellow pixels are observed, in urban and forest regions, we have -  $\lambda_1 > \lambda_2 \approx \lambda_3$ , where eigen are about:  $\lambda_1 \approx 3.3$ ,  $\lambda_2 \approx 0.8$ ,  $\lambda_3 \approx 0.7$ . In the second case, where green pixels are observed, in urban region and radar shadows, we have -  $\lambda_1 \leq \lambda_2 < \lambda_3$ , where:  $\lambda_1 \approx 3.2$ ,  $\lambda_2 \approx 1.3$ ,  $\lambda_3 \approx 0.7$ .

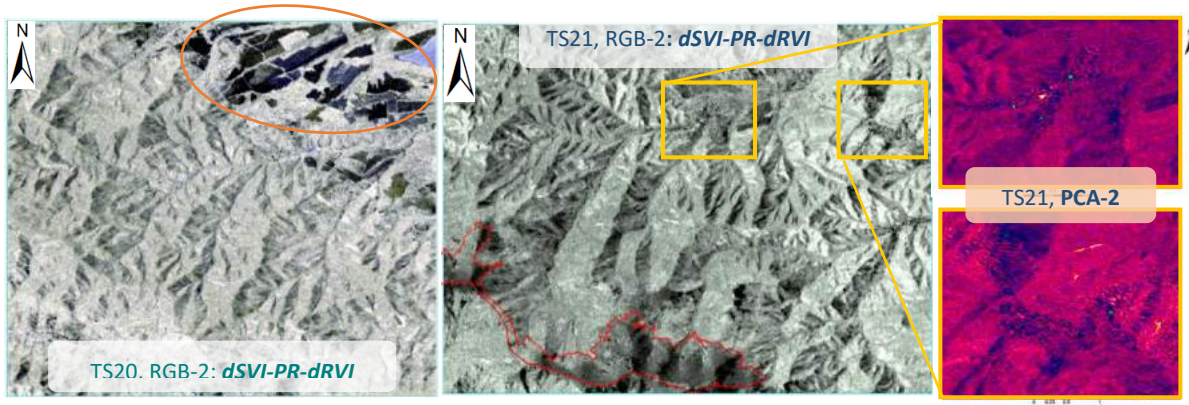


Fig. 14. The RGB-2 (dSVI, PR, dRVI) for both test sites, derived from the  $-\overline{\gamma_{vv}^0}$ , and  $\overline{\gamma_{vh}^0}$ , and showing high correlation in between (greyish), with exception over agricultural areas and reservoir. The PCA-2 on the right, showing differences in urban and within the mountain.

### Regression analysis

In the purpose to study the possible statistical relation between *S1-mean-characteristics* and environmental characteristics (e.g. biomass, relief) regression analysis is considered. Related to that, the following regression tests are performed, aiming different combinations of dependent (DV) versus independent variables (IV) – such as: 1 – IncGeo as DV-1, 2 – TCD as DV-2, 3 – GlobBio/CCI as DV-3; and aiming particular regions of interest – (1) in transect on TS20; (2) for whole scene on TS20/21.

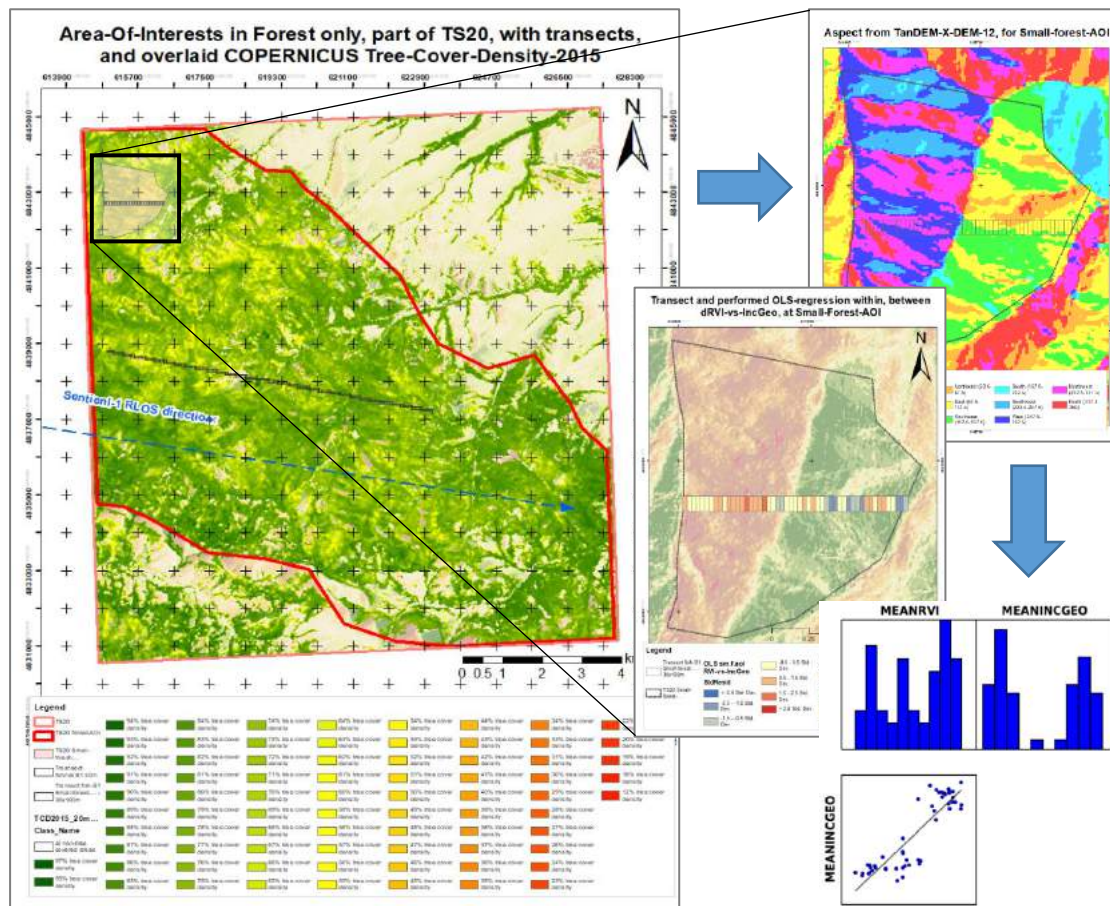


Fig. 15. Thematic map (left) with the two transects over COPERNICUS TCD-2015 base map. Sample maps (two, on the right) of the selected small transect, within quasi-homogenous environment, in terms of slope, aspect, and canopy density, in purpose of the regression test.

**Regression test – 1:** Firstly, the observed correlation between local incidence angle (*IncGeo*) and radar vegetation index (*dRVI*), is taken into account to be statistically tested. For that a small region that constitutes of 51 resolution cells of 30 x 100 m, is located in the NW part of TS20 - “Transect-small”, having high terrain slope, constant incidence angle and aspect, whole with small variations. Statistical distributions and histograms are calculated in transect, followed by single OLS regression in ArcGIS; please, refer to Fig.15. Regression results proves the preliminary observed correlation, between local incidence angle and radar vegetation index with very high coefficient of determination ( $R^2$ ); see, table-6, DV-1. Thereafter, regression over wider transect is performed that constitutes of 196 resolution cells of 50 x 50 m whole over the TS20, aiming regression with DV-1 and 2, where *IncGeo* and *TCD-2015* are considered as dependent variables (see, table-6). Regression result for DV-1 is again high, using multi-parametric regression, but with lower coefficient of determination, because of the larger area used that brings more outliers in statistical point of view. This also points to strong “non-linearity” of the data. Considering the DV-2 combination, shows non statistical correlation between *TCD-2015* and SAR observables, by means of S1-mean-characteristics!

Table 6. Regression results of DV-combinations 1 and 2, with single- and multiple-parametric regression OLS - with the highest correlation result, within the two transects, at TS20

<i>TS20</i>	Transect – small		Transect - big	
<i>DV</i>	Equation tested	$R^2$	Equation tested	$R^2$
1	$IncGeo \sim dRVI_{mean}$	0.7808	$IncGeo \sim dRVI_{mean} + VH_{mean}$	0.6743
2	-	-	$TCD_{2015} \sim dRVI_{mean} + VH_{mean} + VV_{mean}$	0.0724

**Regression test – 2:** For tracking out statistical relationships within whole test area another test is performed, using forest AOI only, determined by the condition:  $TCD-2015 > 10\%$ . Full regression



analysis is performed in that case, using whole DV – combinations mentioned above. Regression equations with the best coefficient of determination are published and analyzed.

Considering local incidence angle, because of the larger region, correlation between *IncGeo* vs. *dRVI* (DV-1) is quite lower but still exists (please, refer to table-7, DV-1/TS20).

Considering regression of *TCD-2015* as dependent variable (DV–2), several equation combinations are approached testing also additional SAR indices and biomass layers as IV. Highest possible correlation in that case is achieved by incorporating the S1-mean-characteristics together with the both biomass layers, pointing out that there is correlative relationship between the tree density and AGB (table-7, DV–2.1/TS21). In spite of that, regression with *GlobBiomass-2010* using same DV gives no statistical correlation, whilst regression with *CCI-biomass-2018* interestingly shows some statistical relationship, with very low coefficient of determination (table-7, DV–2.3/TS21). Regarding *dSVI*, there is no correlation relationship between SAR indices and the tree density (table-7, DV–2.1/TS20).

Considering regression of the biomass layers, using delivered by the Uni-Jena, Lehrstuhl für Fernerkundung – *GlobBiomass-2010* and *CCI-Biomass-2018*, the performed regression shows small differences in depend of the test site environmental conditions. Hence, considering *GlobBiomass*, better result is for TS20, by using cross-pol -  $\gamma_{vh}^0$  (table-7, DV-3.1/TS20) in the equation, rather than -  $\gamma_{vv}^0$  (table-7, DV-3.2/TS20) at the multi-parametric regression, possibly because of the better sensitivity of the cross-pols to the forest volume. It is interesting, that the -  $\overline{dRVI}$  improves regression result, rather than using equation based solely on both polarizations. In spite, the correlative relationship in between is very poor, and does not exists for TS21. For *CCI-Biomass*, also, considering TS20 a kind of correlative relationship exists rather than for TS21, where different IV are found to be valuable for the regression (table-7, DV-3.3/TS20 and TS21). Poorer regression result on behalf of *CCI-Biomass* than *GlobBiomass* is interesting, because reference period for *CCI-Biomass* matches the four years period of the Sentinel-1 - time-series. Nonetheless, could be said that correlative relation between biomass and SAR indices (e.g. *dRVI*, *dSVI*) does not exists, which is proved finally by regressing the *GlobBiomass* versus Polarization Ratio (table-7, DV-3.4/TS21), or by *CCI-Biomass* versus dual-pol SAR vegetation index (table-7, DV-3.5/TS21), despite result of *Pol.Ratio* is better than *dSVI*.

Table 7. Highest correlation results from the regression with whole DV-combinations, including single- and multiple-parametric regression OLS, performed on both test sites

	TS20		TS21	
DV	Equation tested	R <sup>2</sup>	Equation tested	R <sup>2</sup>
1	$IncGeo \sim dRVI_{mean}$	0.4709	-	-
2.1	$TCD_{2015} \sim dSVI_{mean}$	0.0045	$TCD_{2015} \sim VV_{mean} + VH_{mean} + CCI_{Biomass}_{2018} + GlobBiomass_{2010}$	0.2111
2.2	-	-	$TCD_{2015} \sim GlobBiomass_{2010}$	0.0774
2.3	-	-	$TCD_{2015} \sim CCI_{Biomass}_{2018}$	0.1781
3.1	$GlobBiomass_{2010} \sim dRVI_{mean} + VH_{mean}$	0.1528	$GlobBiomass_{2010} \sim VH_{mean} + dRVI_{mean}$	0.0972
3.2	$GlobBiomass_{2010} \sim dRVI_{mean} + VV_{mean}$	0.1482	$GlobBiomass_{2010} \sim VV_{mean} + dRVI_{mean}$	0.0963
3.3	$CCI_{Biomass}_{2018} \sim VH_{mean} + VV_{mean}$	0.1092	$CCI_{Biomass}_{2018} \sim dRVI_{mean} + VV_{mean}$	0.0645
3.4	-	-	$GlobBiomass_{2010} \sim Pol.Ratio_{mean}$	0.0768
3.5	-	-	$CCI_{Biomass}_{2018} \sim dSVI_{mean}$	0.0046
3.6	$CCI_{Biomass}_{2018} \sim GlobBiomass_{2010}$	0.2629	$CCI_{Biomass}_{2018} \sim GlobBiomass_{2010}$	0.3434

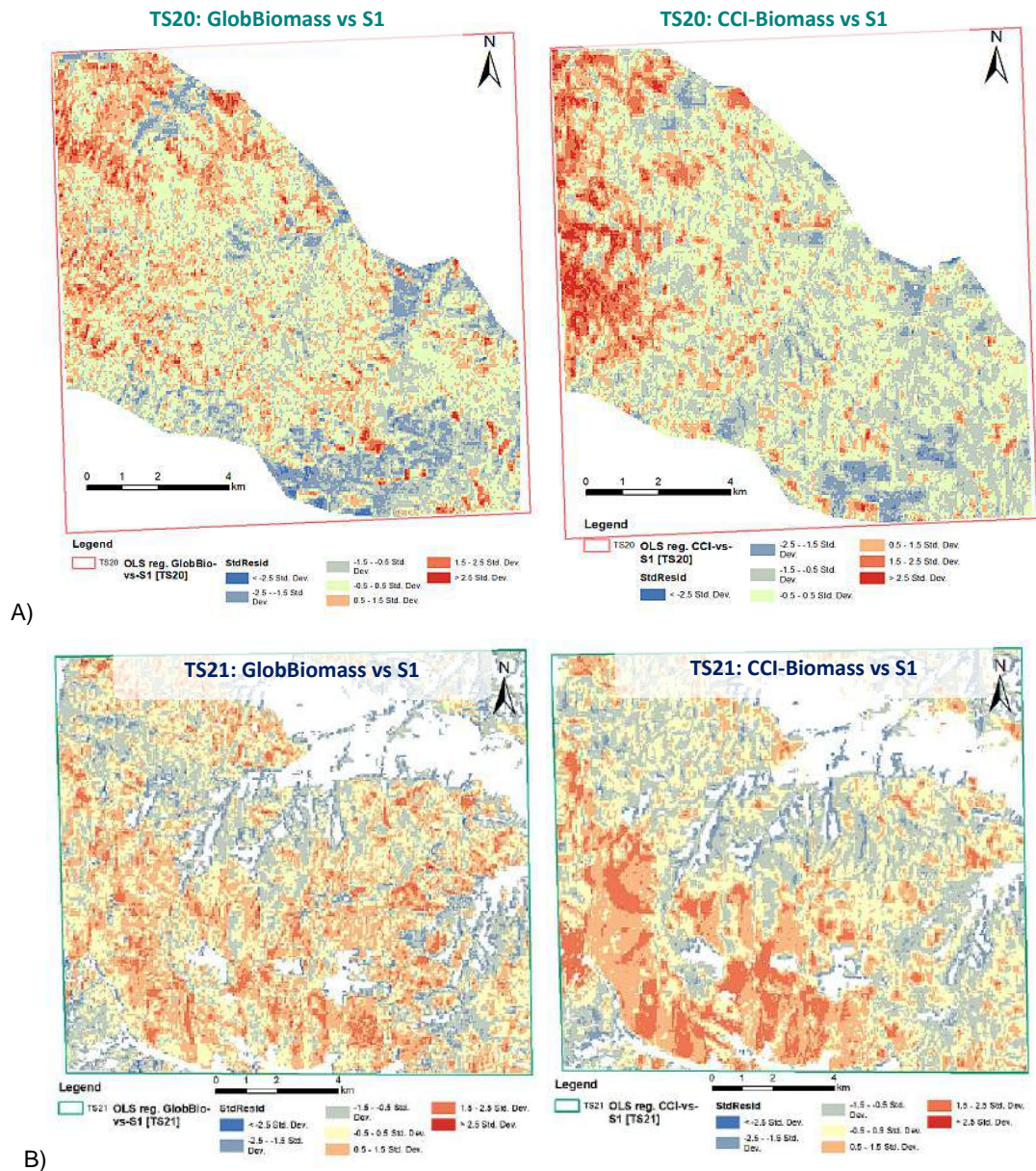


Fig. 16. Residual maps for TS20 (left) and TS21 (right) from multiple-parametric regression using OLS, between GlobBiomass-2010 and CCI-Biomass-2018 vs S1-mean-characteristics, where low statistical correlation is observed in-between

Taking into account geographical representation of the residuals from both OLS-regressions of GlobBiomass and CCI-Biomass versus *S1-mean-characteristics*, could be stated that S1-SAR observables loose sensitivity at regions with high biomass levels, which is expected result, due to fast saturation of the radar backscatter in C-band [9] (see Fig.15 – A). These are residuals with positive distances  $> 1.5$  STD (reddish). Contrariwise, the residuals with negative distances  $< -1.5$  STD (bluish) are dedicated to non-forest areas. Besides, due to differences in AGB estimation by GlobBiomass and CCI-Biomass, residual maps are different, with predominance at CCI-biomass, where distances  $> 2.5$  STD are much more that proofs regression results. In spite, a convergence is observed between low values in dRVI (dark) and high negative distances ( $> 2.5$  STD) at Residual map of GlobBiomass (reddish). Residual map for TS21 confirms stated at the above, about lower sensitivity of the S1-SAR observables at higher levels of AGB, therefore high differences, above  $- 2.0$  STD are observed over southern part of the test site, near BR “Chuprene”.

For finalization of the regression analysis, a correlation between both biomass layers is taken into account. Result showed low correlation inbetween, where higher coefficient of determination is at TS21, unlike the TS20 (see, table-7, DV-3.6). A possible answer to this difference is given from GIS based analysis of calculated AGB- change-layer, where:

$$(4) \Delta AGB = AGB_{GlobBio\_}^{2010} - AGB_{CCI}^{2018}$$

together with the vector information about forest disturbances, from the reference database. A positive convergence is observed for some disturbed forest stands with damages above 30%, together with the AGB-change-layer, and where forest loss is:  $\Delta AGB < -80$  t/ha. That is interesting result, but needs more in depth analysis of those changes, and evaluation of the reference database with forest disturbances. For such utilization, resulted S1-mean-characteristics from the time series are proper tool and could give reliable results. In other hand, this is not the complete answer for the observed changes in AGB, because time difference in between is 8-years and forest is changing, as well as a lot of forestry activities are ongoing in those rural areas.

## Conclusions

To conclude the analysis held in that study, it can be categorically confirm that delineation between deciduous and coniferous forest could be done by means of Sentinel-1 time series intensities products. Utilization of the dual-pol RVI (dRVI) in mountainous temperate forest is of great importance, because it provides that sensitivity to the forest structure. General conclusion is also that geometric distortions influences dRVI, which limitates the correct interpretation in those areas. Thematic analysis via proposed RGB-1: dRVI-VH-VV gives good representation of the backscattering that originates from different type of the scattering media – e.g. land cover. Resulted PCA from RGB-1 gives best delineation between deciduous and coniferous forest type. Additionally tested SAR indices – the dual-pol SVI and Polarization Rati, gives non additional information apart from the dRVI, pointing out to equilibrium of the sensitivity over forest by means of the three tested SAR indices. Contrariwise, this is not the case over other type of natural media, such as agricultural fields and water, where SAR indices differ in-between. The PCA based on RGB-2 provides interesting strong bias at some distinct pixels with strong backscatter toward sensor, colored in yellowish or greenish3h that should be studied.

The resulted supervised classifications that also incorporates Forest type map, resulted with 78.8 and 68.9 overall accuracy for TS20 and TS21 respectively. General uncertainties are dedicated to coniferous forest at BR “Chuprene” (class-7) that constitutes of sloped forest at TS21, whereas crops biased the correct interpretation of grassland on TS21. Coniferous forest in some degree is also misclassified as deciduous forest, mainly in areas where coniferous species are sparse or well mixed up with the deciduous ones. In addition, unsupervised classifications showed better performance in forest edge delineation. Resulted Forest/non-forest masks resulted with high accuracy, where the only frustration is the uncertainty in the foreshortenings.

Subsequent Regression analysis that aimed to test in general statistical correlation between mean characteristics resulted from Sentinel-1 time series, and provided AGB layers from Uni-Jena – GlobBiomass-2010 and CCI-Biomass-2018, as well as the TCD-2015 in the frame of COPERNICUS Services, showed very low or no correlation in between. Most prompt answer about the observed poor correlation between AGB and the SAR observables from Sentinel-1, is the lower saturation level of C-band intensities from forest [9]. Nonetheless, high correlation is observed between dRVI and local incidence angle, with  $R^2 = 0.78$ . Differences in both AGB layers are most likely to be related with the forest loss, due to forest disturbances caused from a past Icethrow disaster event.

Finally, could be stated that conducted utilization of Sentinel-1 time series in mountainous temperate forest, on behalf of dual-polarimetric capabilities, as well as SAR indices in the face of dRVI, gives good results where could be incorporated successfully in variety of thematic analyses for the forest structure, and mapping.

## Acknowledgement

The author would like to acknowledge the University of Jena (FSU-Jena), Lehrstuhl für Fernerkundung about the provided AGB-layers (GlobBiomass-2010 and CCI-Biomass-2018), in the face of Prof. C. Schmullius, P.D. Dr. C. Thiel, and also Felix Cremer and Dr. N. Salepci for the support in the elaboration of the Sentinel-1 - time series. Also to acknowledge DLR about the provided “TanDEM-X DEM12”© in the frame of DEM Proposal. As a final, to acknowledge author’s PhD tutor at SRTI-BAS, Prof. E. Roumenina, and Dr. L. Filchev – head of department.

## References:

1. Fernandez-Ordonez, Y., J. Soria-Ruiz, B. Leblon. "Forest Inventory using Optical and Radar Remote Sensing", Advances in Geoscience and Remote Sensing, ISBN 978-953-307-005-6, 2009, pp. 540–556.
2. Le Toan, T., S. Quegan, M.W.J. Davidson, H. Balzter, P. Paillou, K. Papathanassiou, S. Plummer, F. Rocca, S. Saatchi, H. Shugart, L. Ulander. "The BIOMASS mission: Mapping global forest biomass to better understand the terrestrial carbon cycle", Remote Sensing of Environment 115, 2011, pp. 2850–2860. DOI:10.1016/j.rse.2011.03.020.



3. Lei, Y., P. Siqueira. "Estimation of Forest Height Using Spaceborne Repeat-Pass L-Band InSAR Correlation Magnitude over the US State of Maine", *Remote Sens.*, 6, 2014, pp. 10252–10285. DOI:10.3390/rs61110252.
4. Englhart, S., V. Keuck, F. Siegert. "Aboveground biomass retrieval in tropical forests — The potential of combined X- and L-band SAR data use", *Remote Sensing of Environment* 115, 2011, pp. 1260–1271. DOI:10.1016/j.rse.2011.01.008.
5. Garestier, F., T. Le Toan. "Forest Modeling For Height Inversion Using Single-Baseline InSAR/Pol-InSAR Data", *IEEE TRANSACTIONS ON GEOSCIENCE AND REMOTE SENSING*, VOL. 48, NO. 3, 2010, pp. 1528–1539.
6. Stebler, O., E. Meier, D. Nüsch. "Multi-baseline polarimetric SAR interferometry—first experimental spaceborne and airborne results", *ISPRS Journal of Photogrammetry & Remote Sensing* 56, 2002, pp. 149–166.
7. Ainsworth, T. L., J.P. Kelly, J.-S. Lee. "Classification Comparisons Between Dual-Pol and Quad-Pol SAR Imagery", *Proceedings of ISPRS Journal of Photogrammetry and Remote Sensing*, 64, 2009, pp. 464–471.
8. Banqué, X., J. M. Lopez-Sanchez, D. Monells, D. Ballester, J. Duro, F.Koudogbo. "POLARIMETRY-BASED LAND COVER CLASSIFICATION WITH SENTINEL-1 DATA", *Proceedings of POLinSAR 2015*, ESA, 2015.
9. Imhoff, M. L. "Radar Backscatter/Biomass Saturation: Observations and Implications for Global Biomass Assessment." *Proceeding of the Geoscience and Remote Sensing Symposium, IGARSS'93*. Tokyo, August 18-21, 1993, pp. 43–45. DOI:10.1109/IGARSS.1993.322465.
10. Santoro, M., C. Beer, O. Cartus, C. Schmullius, A. Shvidenko, I. McCallum, U. Wegmüller, A. Wiesmann. "Retrieval of growing stock volume in boreal forest using hyper-temporal series of Envisat ASAR ScanSAR backscatter measurements", *Remote Sensing of Environment* 115, 2011, pp. 490–507.
11. Quegan, S., et al. "GlobBiomass - Algorithm Theoretical Basis Document", D6, GlobBiomass Project ESRIN/Contract No. 4000113100/14/I\_NB, Vol.01, ESA, 2016.
12. Seifert, F., et al. "CCI Biomass Product User Guide v1", *PRODUCT USER GUIDE, YEAR 1, VERSION 1.0*, CCI BIOMASS Project, ESA, 2019.
13. Николов, З., „Около 300 000 кубически метра гори в Северозападна България са засегнати от ледолома в края на миналата година“, *Информация от БТА*, NZ1442BO.020, c/BO/id/1020172, 2015.
14. Mandal, D., V. Kumar, D. Ratha, S. Dey, A. Bhattacharya, J. M. Lopez-Sanchez, H. McNairn, Y. S. Rao. "Dual polarimetric Radar vegetation index for crop growth monitoring using Sentinel-1 SAR data", *Remote Sensing of Environment* 247, 2020, 111954.
16. Small, D., N. Miranda, L. Zuberbühler, A. Schubert. "Terrain-corrected Gamma: Improved thematic land-cover retrieval for SAR with robust radiometric terrain correction", *Proc. 'ESA Living Planet Symposium'*, Bergen, Norway, 28 June – 2 July 2010 (ESA SP-686, December 2010), 2010. DOI: 10.5167/uzh-41236.
17. Truckenbrodt, J, F. Cremer, I. Baris, J. Eberle. "PYROSAR: A FRAMEWORK FOR LARGE-SCALE SAR SATELLITE DATA PROCESSING", *Proc. of the 2019 conference on Big Data from Space (BiDS'19)*, 2019. DOI:10.2760/848593.
18. Cohen, J. "A coefficient of agreement for nominal scale", *Educational Psychological Measure* (20), 1960, 37–46.
19. Congedo, L. „Semi-Automatic Classification Plugin: A Python tool for the download and processing of remote sensing images in QGIS“. *Journal of Open Source Software*, 6(64), 2021, 3172. DOI: <https://doi.org/10.21105/joss.03172>.